Organic Electronics 13 (2012) 114–120

Contents lists available at SciVerse ScienceDirect

Organic Electronics

journal homepage: www.elsevier.com/locate/orgel

Optimization of the side-chain density to improve the charge transport and photovoltaic performances of a low band gap copolymer

Laure Biniek [a], Sadiara Fall [b], Christos L. Chochos [a], Nicolas Leclerc [a,*], Patrick Lévêque [b], Thomas Heiser [b]

[a] Laboratoire d'Ingénierie des Polymères pour les Hautes Technologies, Université de Strasbourg, Ecole Européenne de Chimie, Polymères et Matériaux, 25 rue Becquerel, 67087 Strasbourg, France
[b] Institut d'Electronique du Solide et des Systèmes, Laboratoire Commun UdS-CNRS, UMR 7163, 23 rue du Loess, 67037 Strasbourg, France

ARTICLE INFO

Article history:
Received 12 September 2011
Received in revised form 14 October 2011
Accepted 18 October 2011
Available online 1 November 2011

Keywords:
Low band-gap
Molecular weight
Processability
Charge carriers mobility
Bulk heterojunction

ABSTRACT

Poor processability and low molecular weights are often hindering the efficient utilization of novel conjugated polymers in optoelectronic devices. Increasing the alkyl side-chain density generally enhances the polymer solubility but may affect as well its optoelectronic properties. In this work, we use density functional theory to identify ways to increase the side-chain density of donor–acceptor alternate copolymers based on 2,1,3-benzothiadiazole, thiophene and thieno[3,2-*b*]thiophene units, without modifying there otherwise promising frontier orbital energy levels. Following the theoretical results, a new polymer could be synthesized, exhibiting good processability and improved charge transport. As a consequence, the photovoltaic device performances of this polymer family could be enhanced, reaching a 3.7% power conversion efficiency in a standard device configuration and without any post-deposition treatment.

1. Introduction

Organic photovoltaic (OPV) solar cells are promising candidates for future low-cost renewable energy production. In particular, donor–acceptor bulk heterojunction (BHJ) polymer-fullerene devices, processed from solution, have attracted a lot of attention and have seen their power conversion efficiency increase continuously over the last few years [1]. Synthesis of new low-band-gap conjugated polymers, acting as electron donors, has contributed significantly to this progress. The target properties that the polymer should possess are now well established: a deep-lying HOMO level for a high open-circuit voltage (V_{oc}) [2], a band-gap close to 1.5 eV for optimum light harvesting [3], and a charge carrier mobility of the order of 10^{-3} $cm^2/V/s$ for efficient charge extraction are highly desirable [2b]. Planar conjugated backbones that allow strong π–π stacking interactions are often considered as particularly promising, since these interactions minimize the energy barrier for charge hopping and lead to high carrier mobilities. However, planar molecules also tend to aggregate in solution and therefore may suffer from low solubility in common solvents. The latter property leads to poor processability and impedes the synthesis of high molecular weight polymers. Yet, it has been shown on other conjugated systems, that higher molecular weights often lead to better charge transport and OPV device performances [4,5].

The polymer solubility is generally controlled by the introduction of alkyl side-chains. The latter molecular design is however non-trivial. Due to steric interactions, the side-chains may perturb the conjugated backbone planarity and alter the desired polymer opto-electronic properties. They may also influence the polymer – fullerene interactions, thereby modifying the polymer:fullerene blend morphology as well as the optimum polymer:

* Corresponding author. Tel.: +33 (0) 368 852 709; fax: +33 (0) 368 852 716.
E-mail address: leclercn@unistra.fr (N. Leclerc).

1566-1199/$ - see front matter © 2011 Elsevier B.V. All rights reserved.
doi:10.1016/j.orgel.2011.10.011

fullerene mass ratio (i.e. the blend composition that leads to the best PV performances) [6]. In a recent work on a new copolymer family called PTBzT^2 (see below), consisting of an alternation of electron deficient 2,1,3-benzothiadiazole units and electron rich thiophene and thieno[3,2-*b*]thiophene units, we have shown that the optical band-gap may be varied by more than 0.3 eV, the hole mobility by orders of magnitude and the photovoltaic efficiency by a factor of ten for a given polymer:fullerene ratio, solely by changing the alkyl chain nature (from linear to branched) or grafting position [7]. Also the optimum polymer:fullerene ratio varied from 1:4 to 1:1, when switching from linear to branched side chains. The PTBzT^2-CEHβ copolymer (see Fig. 2) was particularly promising, with an optical band-gap of 1.56 eV, an ionization potential of 5.0 eV and a hole mobility of 10^{-3} cm^2/V/s (measured on the high molecular weight fraction) [7]. Yet, the power conversion efficiency (2.7%) of OPV devices obtained using a PTBzT^2-CEHβ:PCBM (1:1) blend, although significant for a new polymer material, was below our expectation. A possible cause for this limited efficiency was the fact that only the chloroform fraction, with a relatively low molecular weight (M_n = 3000 g/mol), was soluble enough to allow the elaboration of an operational photovoltaic device. We therefore started to explore possible ways to synthesis a polymer with similar frontier orbitals than PTBzT^2-CEHβ but with a higher solubility and molecular weight.

Here, we investigate methods to increase the alkyl chain density (number of side chains per repeating unit) on copolymers of the same family. We use density functional theory to calculate changes in the molecular conformation induced by each method. Taking into account of the theoretical results, we succeeded to synthesize a new copolymer with a higher molecular weight and similar frontier orbitals than PTBzT^2-CEHβ but with improved charge transport. As a consequence, a power conversion efficiency of 3.7% could be reached using a conventional device structure without thermal or solvent annealing treatments.

2. Experimental section

2.1. Materials synthesis and characterizations

^{1}H and ^{13}C NMR spectra were recorded on a Bruker 300 UltrashieldTM 300 MHz NMR spectrometer and a Bruker 400 UltrashieldTM 400 MHz NMR spectrometer, with an internal lock on the 2H-signal of the solvent ($CDCl_3$).

Size exclusion chromatography (SEC) measurements were performed with a Waters Alliance GPCV 2000 instrument (Milford/MA) that incorporate a differential refractive index and a viscosimeter. 1,2,4 Trichlorobenzene (TCB) was used as the mobile phase at a flow rate of 1 mL min^{-1} at 150 °C. It was stabilized with 2,6-di(tert-butyl)-4-methylphenol. All polymers were injected at a concentration of 1 mg mL^{-1}. The separation was carried out on three agilent columns (PL gel Olexis 7 × 300 mm) and a guard column (PL gel 5 μm). Columns and detectors were maintained at 150 °C. The Empower software was used for data acquisition and data analysis. The molecular weight distributions were calculated with a calibration curve based on narrow polystyrene standards (from Polymer Standard Service, Mainz), using only the refractometer detector. UV–visible absorption spectroscopy measurements were done using a Shimadzu UV-2101 spectrophotometer. The absorption spectra were measured on both, *o*-DCB polymer solutions and polymer thin films spin-coated on glass substrates.

Cyclic voltammetry analyzes were carried out with a BioLogic VSP potentiostat using platinum electrodes at a scan rate of 20 mV/s. The measurements were performed on polymer thin film drop-casted from *o*-DCB solutions onto a platinum working electrode. A Pt wire was used as counter electrode and Ag/Ag$^+$ as reference electrode in a 0.1 mol L^{-1} solution of tetrabutylammonium perchlorate in acetonitrile. Ferrocene was used as internal standard to convert the values obtained with Ag/Ag$^+$ reference to the saturated calomel electrode scale (SCE).

The synthesis of 4,7-bis(5-bromo-3-(2-ehtylhexyl) thiophen-2-yl)-2,1,3-benzothiadiazole **(1)**, 2-(trimethylstannyl)-4-(2-ethylhexyl)thiophene **(2)**, and 2-5-bis-trimethylstannyl-thieno[3,2-*b*]thiophene **(5)** have been described in our previous work [8]. Toluene (ACS grade) was distilled over sodium prior to use. All other chemicals were purchased from Aldrich and used without further purification.

2.2. Synthesis

The monomers synthesis is sketch in the Fig. 1.

2.2.1. 4,7-bis(3′,4-di(2-ethylhexyl)-2,2′-bithiophen-5-yl)-2,1,3-benzothiadiazole *(3)*

2-(trimethylstannyl)-4-(2-ethylhexyl)thiophene **(2)** (3 eq.) and 4,7-bis(5-bromo-3-(2-ehtylhexyl)thiophen-2-yl)-2,1,3-benzothiadiazole **(1)** (1 eq.) were dissolved in dry toluene (0.1 M). Then, $Pd(PPh_3)_4$ in catalytic amount was added and the reaction mixture was stirred at 110 °C for 24 h under argon atmosphere. Then, the reaction mixture was filtered through a pad of celite and the toluene solution was evaporated and dried under high vacuum. The crude product was purified by column chromatography on silica gel with cyclohexane as eluent providing a red oil. (Yield: 56%) ^{1}H NMR (300 MHz, $CDCl_3$, ppm): δ = 7.96 (s,1H), 7.84 (s, 1H), 7.06 (s, 1H), 6.92 (s,1H), 2.80 (d, 2H, ^3J = 7.2 Hz), 2.58 (d, 2H, ^3J = 6.8 Hz), 1.76 (m, 1H), 1.62 (m, 1H), 1.31 (m, 16H), 0.90 (m, 12 H). ^{13}C NMR (75 MHz, $CDCl_3$, ppm): δ = 152.63, 142.39, 139.46, 136.52, 135.45, 133.45, 131.11, 128.25, 125.53, 125.19, 121.27, 40.39, 40.18, 34.59, 33.60, 32.56, 28.95, 25.75, 25.65, 23.11, 23.05, 14.13, 10.88, 10.74.

2.2.2. 4,7-Bis(5′-bromo-3,4′-bis(2-ethylhexyl)-[2,2′-bithiophen]-5-yl)benzo[c][1,2,5] thiadiazole *(4)*

Compound **(3)** (1 eq.) was solubilized in $CHCl_3$ (0.15 M) and acetic acid (0.15 M) under argon in the dark. NBS (2 eq.) was added portionwise. The resulting solution was stirred at room temperature under argon overnight. Water and diethylether were added and the resulting solution was stirred for 2 h. The organic phase was separated from the water phase and extracted with brine (3 × 100 mL).

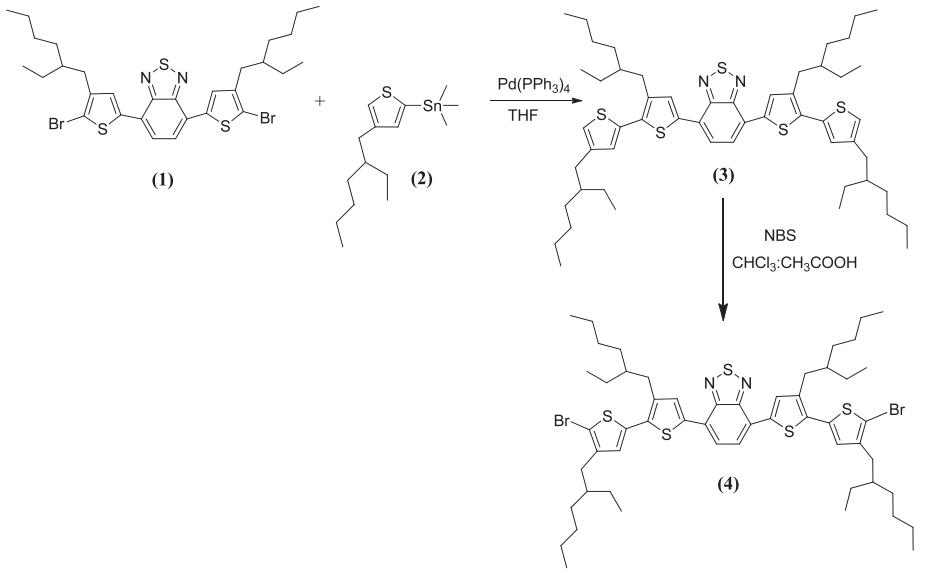

Fig. 1. Monomers synthesis.

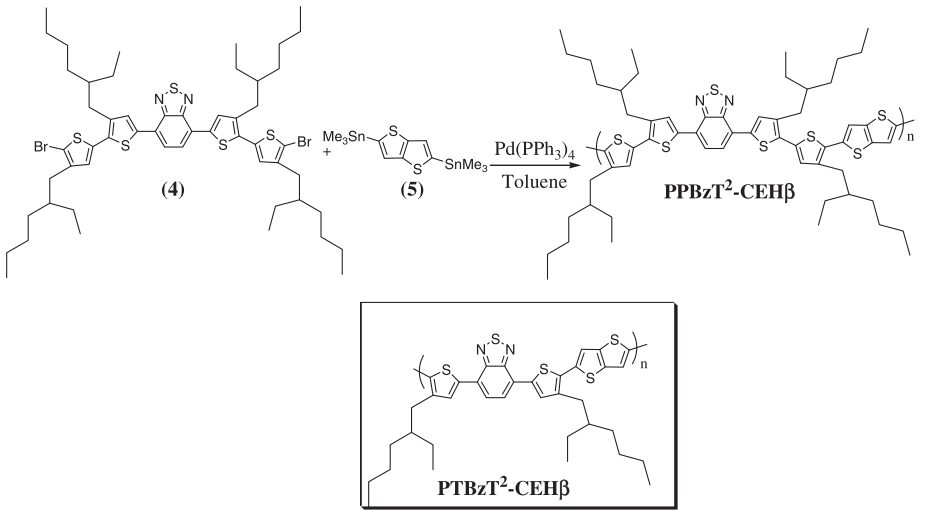

Fig. 2. Synthesis and molecular structure of PPBzT^2-CEHβ. The structure of PTBzT^2-CEHβ is also presented (inset).

The organic phase was dried with sodium sulfate, filtered and the solvent evaporated under reduced pressure and further dried under high vacuum. The crude product was purified by column chromatography on silica gel with cyclohexane as eluent. (Yield: 79%). ^{1}H NMR (300 MHz, $CDCl_3$, ppm): δ = 7.94 (s, 1H), 7.83 (s, 1H), 6.92 (s, 1H), 2.86 (d, 2H, ^3J = 7.2 Hz), 2.54 (d, 2H, ^3J = 7.2 Hz), 1.73 (m, 2H), 1.32 (m, 16H), 0.91 (m, 12H). ^{13}C NMR (75 MHz, $CDCl_3$, ppm): δ = 152.56, 141.72, 140.01, 137.00, 135.31, 132.42, 131.00, 127.79, 125.49, 125.25, 109.69, 40.25, 40.01, 33.83, 33.62, 32.55, 28.84, 28.69, 26.90, 25.78, 25.75,2309, 23.06, 14.12, 10.85, 10.77. Elemental analysis found: C, 61.40; H, 7.24; Br, 14.05; N, 2.48; S, 13.54. Calc. for $C_{54}H_{74}Br_2N_2S_5$: C, 60.54; H, 6.96; Br, 14.92; N, 2.61; S, 14.97.

2.2.3. Polymerization of ***PPBzT^2-CEHβ***

Thieno[3,2-*b*]thiophene derivative **(5)** (1 eq.) and compound **(4)** (1 eq.) were dissolved in dry toluene (0.02 M). Then, $Pd(PPh_3)_4$ (0.02 eq.) was added and the reaction mixture was stirred at 110 °C under argon atmosphere for 17 h. Then, the toluene solution was evaporated, the mixture was solubilized in $CHCl_3$. The polymer was purified by precipitation in methanol, filtered and washed on Soxhlet apparatus with methanol, cyclohexane, chloroform and *o*-DCB. The chloroform and then the *o*-DCB fraction were evaporated under reduced pressure and the polymer was precipitated in methanol, filtered and finally dried under high vacuum, providing a film with a metallic shine with 88% of yield. ^{1}H NMR (300 MHz, $CDCl_3$, ppm): δ = 7.98 (s, 1H), 7.84 (s, 1H), 7.32 (s,1H) 7.10 (s, 1H), 2.85

(m, 2H), 2.79 (m, 2H), 1.78 (m, 2H), 1.97 (m, 16H), 0.91 (m, 12H).

The thermal stability of the polymer has been evaluated through thermal gravimetric analysis showing a decomposition temperature of 211 °C (5% weight loss).

2.3. Computational study

In order to anticipate the influence of the alkyl side chain positioning on the copolymer optoelectronic properties, density functional theory at the B3LYP/6-311+G* level of theory in vacuum (using Spartan 10) [9] was utilized to model the structural and electronic properties of relevant molecular structures. In particular, the HOMO and LUMO level positions and related electron distributions were calculated. To keep the computational time within a reasonable range, the alkyl chains were replaced by methyl groups. It is thereby assumed that the electronic coupling between alkyl chains and the π-electron system is negligible. CH_3 groups were placed at both ends and the dihedral angle between the last carbon atom and the methyl group was kept fixed in order to mimic the rigidity of the actual polymer.

2.4. OFET and SCLC devices fabrication and characterization

Bottom contact field-effect transistors (FETs) were elaborated on commercially available pre-patterned test structures whose source and drain contacts were composed of 30 nm thick gold and 10 nm thick Indium Tin Oxide (ITO) bilayers. A 230 nm thick silicon oxide was used as gate dielectric and n-doped ($3 \times 10^{17}/cm^3$) silicon crystal as gate electrode. The channel length and channel width were 20 μm and 10 mm, respectively. The test structures were cleaned in acetone and isopropyl alcohol and subsequently for 15 min in an ultra-violet ozone system. Then, hexamethyldisilazane (HMDS) was spin-coated (500 rpm for 5 s and then 4000 rpm for 50 s) under nitrogen ambient and followed by an annealing step at 130 °C for 5 min. Finally, 4 mg/mL anhydrous *o*-DCB polymer solutions were spin-coated (1250 rpm for 60 s and 2000 rpm for 120 s) to complete the FET devices. The samples were then left overnight under vacuum ($<10^{-6}$ mbar) to remove residual solvent traces. Both, the FET elaboration and characterizations were performed in nitrogen ambient. Space charge limited current (SCLC) hole only devices were elaborated and characterized to estimate the hole mobility in PTBzT^2-CEHβ and **PPBzT^2-CEHβ** in the direction perpendicular to the substrate. The SCLC device structure was: ITO/PEDOT:PSS(∼40 nm)/polymer/PEDOT:PSS/Al(∼120 nm) using the photovoltaic device fabrication described below for the substrate cleaning and polymer deposition procedure. After deposition of the top PEDOT:PSS layer (spin coated), the SCLC devices were dried under vacuum at 110 °C for 15 min before thermal evaporation of Al to ensure an accurate electrical contact. For each polymer, several thicknesses ranging from 80 to 200 nm were tested in order to rule out injection problems at the PEDOT:PSS/polymer interface. The hole mobility was extracted using the standard expression for charge space limited current including a field dependent expression for the mobility [10].

2.5. Photovoltaic device fabrication and characterization

Bulk heterojunction devices were elaborated using **PPBzT^2-CEHβ** as electron donor and $PC_{60}BM$ as electron acceptor. The standard device structure was the following: ITO/PEDOT:PSS(∼40 nm)/polymer:PCBM(∼100 nm)/Al(∼120 nm). Indium tin oxide coated glass with a surface resistance lower than 20 Ω/sq was used as transparent substrate. ITO was cleaned sequentially by ultrasonic treatments in acetone, isopropyl alcohol, and deionized water. After an additional cleaning for 30 min under ultra-violet generated ozone, a highly conductive polyethylene dioxythiophene:polystyrene-sulfonate PEDOT:PSS was spin coated (1500 rpm: 40 nm) from an aqueous solution and dried for 30 min at 120 °C under vacuum before being transferred to the nitrogen filled glove box. The dichlorobenzene polymer:PCBM solutions were stirred at 70 °C for 48 h before spin-coating. Unless otherwise stated, the solution had a total concentration of 40 mg/mL with a polymer:fullerene weight fraction ranging from 1:1 to 1:4. Finally, a 120 nm thick aluminum layer was thermally evaporated and used as cathode. The device active area was 9 mm^2, while each sample included four independent diodes. With the most promising polymer an extra series of devices was elaborated with an additional Ca (20 nm) layer between the active layer and the aluminum cathode. Current density vs. voltage (*J*–*V*) characteristics were measured under darkness and under AM1.5 (100 mW/cm^2) illumination using an Oriel 150 W solar simulator.

3. Results and discussion

The molecular structure of the copolymer PTBzT^2-CEHβ, which has led previously to our best performing devices on this polymer family [7], is given as an inset in Fig. 2. The acronym "PTBzT^2" refers to a polymer (P) which is formed by the alternation of a trimer (T), derived from a central 2,1,3-benzothiadiazole (Bz) unit surrounded by two alkylthiophene units, and a thieno[3,2-*b*]thiophene (T^2) unit. The acronym extension highlights the side chain nature and positioning: CEH corresponds to 2-ethylhexyl alkyl chains, whereas the β index designates chains that are in the 4th position.

As stated above, the poor solubility of the highest molecular weight fraction (M_n = 11,000 g/mol) of PTBzT^2-CEHβ impeded the formation of homogeneous films. A higher side-chain density is likely to enhance the polymer solubility but may as well change its optoelectronic properties. Two synthetic strategies may be followed to increase the chain density: by grafting additional alkyl chains on either the 2,1,3-benzothiadiazole or the thieno[3,2-*b*]thiophene units, or by adding two alkylthiophene units to the copolymer donor block.

Density functional theory calculations using Spartan 10 [9] have been performed to evaluate the expected impact of the different grafting positions or extra alkylthiophene units on the dihedral angles between the aromatic units and consequently on the optoelectronic properties of the copolymer. The general structure that has been considered for calculations is shown in Fig. 3 where the anchoring

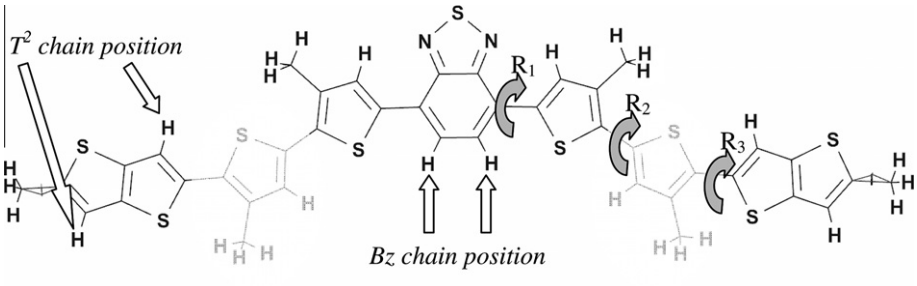

Fig. 3. Molecular structure used for the computational study. The positions of the alkyl chains added on the PTBzT^2 backbone are indicated by the arrows while the light gray alkylthiophene units correspond to PPBzT^2-CEHβ. The calculated dihedral angles are also drawn on the scheme.

Table 1
Calculated dihedral angles and corresponding HOMO and LUMO levels.

Polymer	R_1 (°)	R_2 (°)	R_3 (°)	HOMO (eV)	LUMO (eV)
PTBzT^2-CEHβ	1–2	–	16–18	−4.71	−2.68
PPBzT^2-CEHβ	2–3	18–20	28–30	−4.70	−2.68
Bz-anchoring	56–58	–	29–31	−4.88	−2.31
T^2-anchoring	7–9	–	56–58	−5.05	−2.63

positions (Bz or T^2 anchoring) are indicated by arrows and the extra alkylthiophene are drawn in gray (**PPBzT^2-CEHβ**). The dihedral angles are also shown. It should be noted that the dihedral angle R_2 exists only for the molecule with additional thiophene units. To keep the computational time within a reasonable range, the alkyl chains were replaced by methyl groups. The calculated dihedral angles and frontier orbital levels are reported in Table 1. The values obtained for the PTBzT^2-CEHβ-like model molecule are given as a reference.

Steric hindrance induced by the addition of alkyl chains on the 2,1,3-benzothiadiazole unit is found to have a strong impact on the R_1 angle, while the addition of alkyl chains on the thieno[3,2-*b*]thiophene unit increases mostly R_3. In both cases the π-orbital overlap between neighboring aromatic units is reduced, leading to changes in the frontier orbital energy levels and, more specifically, to a larger energy band-gap. Note that due to the small number of aromatic cycles taken into account by the model, the absolute energy values are not reliable. Only relative changes of the HOMO and LUMO values with respect to the reference molecule, are meaningful. The results obtained for the Bz position are in agreement with the UV–visible absorption measurements performed by Zhou et al. on another low-band gap copolymer having solubilizing side-chains positioned on the benzothiadiazole units [11].

On the other hand, only a minor increase in R_3 is observed after the addition of two extra alkylthiophene units to the copolymer donor block. Also the frontier energy level positions are close to those of the reference molecule. Taking into account these considerations, we decided to insert two additional alkylthiophene units, with 2-ethylhexyl side chains on the 4-position of the thiophene ring, into the conjugated backbone, leading to a new pentamer-based copolymer called **PPBzT^2-CEHβ**. The ethylhexyl chain density was thereby increased from 2 per monomer in PTBzT2-CEHβ to 4 per monomer in **PPBzT^2-CEHβ**.

In the following, the synthesis procedure, the material characterization, the charge transport and photovoltaic properties of the pentamer-based oligothiophene copolymer are presented and compared to the PTBzT^2-CEHβ trimer-based copolymer.

The synthesis of **PPBzT^2-CEHβ** is shown in Fig. 2. The detailed procedures for the monomer and polymer synthesis are described in the experimental part (see also Fig. 1). The pentamer-based monomer (4) has been obtained via a Stille coupling reaction between 2-(trimethylstannyl)-4-(2-ethylhexyl)thiophene and 4,7-bis(5-bromo-4-(2-ethylhexyl)thiophen-2-yl)-2,1,3-benzothiadiazole and subsequently dibrominated using *N*-bromosuccinimide (NBS) agent. **PPBzT^2-CEHβ** was synthesized by a Stille coupling reaction using Pd(PPh$_3$)$_4$ as catalyst and toluene as solvent. In order to investigate the influence of the alkyl side chain density on the solubility, the **PPBzT^2-CEHβ** polymerization conditions (polymerization time and solution concentration) were kept identical to those previously used for PTBzT^2-CEHβ. The molecular weight of the polymer was estimated by gel permeation chromatography in hot trichlorobenzene. The highly soluble chloroform fraction of **PPBzT^2-CEHβ** exhibited a higher molecular weight (M_n = 12,000 g/mol, PDI = 1.5) than the corresponding chloroform fraction of PTBzT^2-CEHβ (M_n = 3000 g/mol, PDI = 1.3), giving evidence for the better solubility of the pentamer-based polymer. Unfortunately, the *ortho*-dichlorobenzene fraction of **PPBzT^2-CEHβ** has not been characterized by SEC due to its low solubility even in hot trichlorobenzene. However, we may consider that the molecular weight should be higher than 12,000 g/mol. In the following of this paper, only the soluble chloroform fraction of **PPBzT^2-CEHβ** will be studied and discussed.

The UV–Vis absorption spectra of the chloroform fraction of **PPBzT^2-CEHβ** in *o*-DCB solution and in spin coated thin films are shown in Fig. 4 and compared to results previously obtained on PTBzT^2-CEHβ [7]. Both absorption

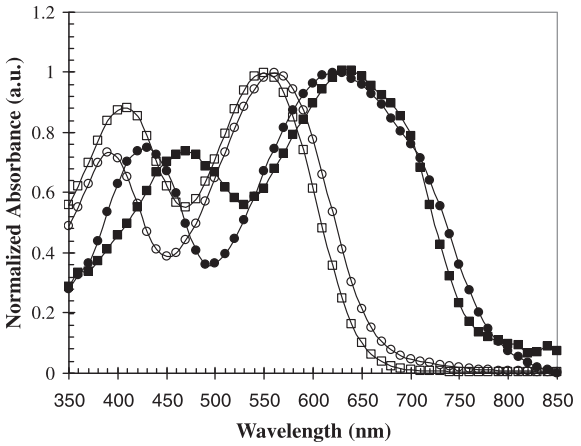

Fig. 4. Normalized absorption spectra of PTBzT^2-CEHβ (circles) and PPBzT^2-CEHβ (squares) in *o*-DCB solution (open symbols) and in thin films (closed symbols).

spectra exhibit two distinct optical absorption bands, similar to those commonly observed in other donor–acceptor based copolymers. The solution spectrum of **PPBzT^2-CEHβ** contains two absorption maxima at 406 and 550 nm, respectively. Increasing the conjugation length of the donor block of the copolymer results in a slight bathochromic shift of the high energy transition (+13 nm) and a hypsochromic shift of the low energy transition (−11 nm). A similar tendency has been observed before by Reynolds et al. [12] on other donor–acceptor copolymers and has been attributed to the decreasing relative concentration of the electron deficient unit (2,1,3-benzothiadiazole) along the polymer backbone. In solid state, the absorption spectrum of **PPBzT^2-CEHβ** displays two absorption peaks at 471 and 626 nm. Those peaks are red-shifted by more than 65 nm in comparison to the corresponding solution spectrum, indicating the presence of strong intermolecular – interactions. The optical band gaps deduced from the absorption onsets in the solid state are 1.62 eV and 1.56 eV for **PPBzT^2-CEHβ** and PTBzT^2-CEHβ, respectively. These relatively close values point out that the extra branched alkylthiophenes have only a minor influence on the polymer conjugation length and intermolecular interactions.

The HOMO and LUMO levels have been measured by cyclic voltammetry in solid state. Only the oxidation wave could be observed for **PPBzT^2-CEHβ** with an oxidation potential onset of 0.64 V vs. SCE and a HOMO level situated at −5.04 eV similar to the one measured for the trimer-based polymer (−5.00 eV). Again, the addition of the two more branched alkylthiophene units has a limited influence on the electrochemical properties of the copolymers.

The charge transport in **PPBzT^2-CEHβ** (chloroform fraction) was first investigated by using field-effect transistors in a bottom contact configuration. The hole mobility in the saturation regime was found to be 2×10^{-3} cm^2/V/s. This value is one order of magnitude higher than the hole mobility of PTBzT^2-CEH (chloroform fraction, $\mu_h = 2 \times 10^{-4}$ cm^2/V/s, $M_n = 3$ kg/mol) [7] but is comparable to the value measured on the *o*-DCB fraction of PTBzT^2-CEH after Soxhlet extraction ($\mu_h = 1 \times 10^{-3}$ cm^2/V/s $M_n = 12$ kg/mol). These results point out firstly that the carrier mobility increases with molecular weight as expected, similar to what has been observed for other conjugated polymers [6c–d] and secondly that the addition of two more alkylthiophene units into the conjugated backbone does not influence significantly the hole mobility for comparable molecular weights. Hole mobility was also extracted in the direction perpendicular to the substrate using SCLC hole only devices. The SCLC hole mobility was 3×10^{-5} cm^2/V/s and 2×10^{-5} cm^2/V/s for the *o*-DCB fraction of PTBzT^2-CEHβ ($M_n = 12$ kg/mol) and for the chloroform fraction of **PPBzT^2-CEHβ** ($M_n = 12$ kg/mol), respectively. As often observed, the SCLC hole mobility is lower than the OFET hole mobility for each polymer. On the other hand, for comparable molecular weights, the trimer based and pentamer based polymers exhibit similar hole mobilities. Hole mobilities measured by OFET and SCLC are reported in Table 2.

The photovoltaic properties of the new polymer were investigated by preparing PPBzT^2-CEHβ:PC$_{61}$BM photovoltaic devices. As for the trimer-based copolymer [7], the most efficient devices were also obtained for a 1:1 copolymer:PC$_{61}$BM ratio. The simplified device structure ITO/PEDOT:PSS/active layer/Al was used first in order to facilitate

Table 2
Molecular weights and hole mobilities of PTBzT^2-CEHβ and PPBzT^2-CEHβ.

		M_n (g/mol)	E_g (eV)[a]	μ_h-OFET (cm^2/V/s)	μ_h-SCLC (cm^2/V/s)
PTBzT^2-CEHβ	$CHCl_3$ fraction	3000	1.56	2×10^{-4}	–
	o-DCB fraction	12,000		1×10^{-3}	3×10^{-5}
PPBzT^2-CEHβ	$CHCl_3$ fraction	12,000	1.62	2×10^{-3}	2×10^{-5}

[a] Optical band gaps measured from UV–visible spectra.

Table 3
Best photovoltaic parameters obtained for copolymer:PC$_{61}$BM blends (weight ratio 1:1).

	Cathode	V_{oc} (V)	J_{sc} (mA/cm^2)	FF (%)	PCE (%)
PTBzT^2-CEHβ[a]	Al	0.58	5.7	45	1.5
PPBzT^2-CEHβ	Al	0.63	11.3	45	3.2
	Ca/Al	0.66	10.7	52	3.7

[a] The results on trimer-based polymer are from [7].

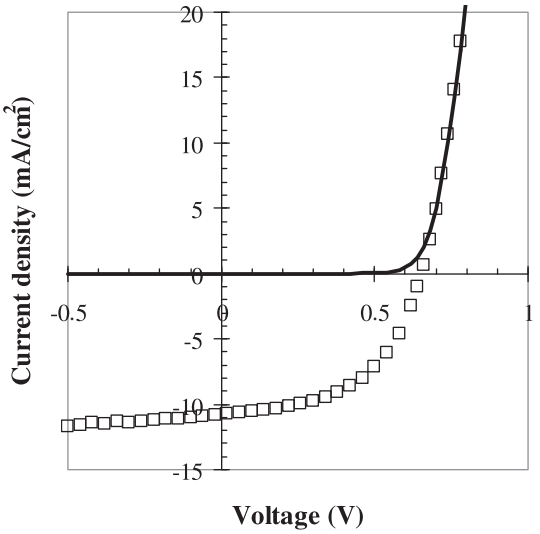

Fig. 5. Current density vs. Voltage (J–V) characteristics for a PPBzT^2-CEHβ device in the dark (continuous line) and using standard AM1.5 (100 mW/cm^2) illumination conditions (open squares).

comparison with previous results obtained with PTBzT^2-CEH. The best photovoltaic parameters are listed in Table 3.

As expected from the similar HOMO level positions, the device open-circuit voltage (V_{oc}) is close to that of PTBzT^2-CEHβ based devices (given in Table 3 for comparison). On the other hand, the short circuit current density (J_{sc}) is almost a factor of two higher than that of PTBzT^2-CEHβ devices and leads to a two-fold increase in the power conversion efficiency. We attribute this significant increase to the higher charge carrier mobility in **PPBzT^2-CEHβ**. It is worth mentioning that these results were obtained without any pre- or post-deposition thermal annealing or solvent annealing treatments.

In order to further investigate the potential of **PPBzT^2-CEHβ** as electron donor material, we elaborated devices using a Ca (20 nm)/Al bilayer as cathode. As a consequence, the fill factor could be improved significantly and led to a promising PCE of 3.7% using pristine PPBzT^2-CEHβ:PC$_{61}$BM devices (Fig. 5). This result highlights the interest of this polymer for photovoltaic applications and substantiates the relevance of further, up-coming, device optimizations.

4. Conclusion

The present work shows that the addition of alkylthiophene units into the donor moiety of low-band gap donor–acceptor copolymers based on electron deficient 2,1,3-benzothiadiazole units and electron rich thiophene and thieno[3,2-*b*]thiophene units allows to enhance the polymer solubility and molecular weight without affecting significantly the π-orbitals. As a result, polymers with a better processability and charge transport could be synthesized and the photovoltaic device performances improved significantly.

Acknowledgements

The authors acknowledge the financial support from the Région Alsace (PMNA jeunes chercheurs) and from the PIE-CNRS program. Nicolas Zimmermann and Caroline Eckert are acknowledged for their help in device elaboration.

References

[1] P.-L.T. Boudreault, A. Najari, M. Leclerc, Chem. Mater. 23 (2011) 456–469.
[2] (a) S. Wen, J. Pei, Y. Zhou, P. Li, L. Xue, Y. Li, B. Xu, W. Tian, Macromolecules 42 (2007) 4977;
(b) M.C. Scharber, D. Mühlbacher, M. Koppe, P. Denk, C. Waldauf, A.J. Heeger, C.J. Brabec, Adv. Mater. 18 (2006) 789–794.
[3] W. Shockley, H.J. Queisser, J. Appl. Phys. 32 (1961) 510–519.
[4] (a) S. Wakim, S. Beaupré, N. Blouin, B.-R. Aich, S. Rodman, R. Gaudiana, Y. Tao, M. Leclerc, J. Mater. Chem. 19 (2009) 5351–5358;
(b) J.K. Jin, J.K. Choi, B.J. Kim, H.B. Kang, S.C. Yoon, H. You, H.T. Jung, Macromolecules 44 (2011) 502–511;
(c) H.N. Tsao, D.M. Cho, I. Park, M.R. Hansen, A. Mavrinskiy, D.Y. Yoon, R. Graf, W. Pisula, H.W. Spiess, K. Müllen, J. Am. Chem. Soc. 133 (2011) 2605–2612;
(d) A. Zen, M. Saphiannikova, D. Neher, J. Grenzer, S. Grigorian, U. Pietsch, U. Asawapirom, S. Janietz, U. Scherf, I. Lieberwirth, G. Wegner, Macromolecules 39 (2006) 2162–2171.
[5] M. Brinkmann, P. Rannou, Macromolecules 42 (2009) 1125–1130.
[6] (a) E. Wang, M. Wang, L. Wang, C. Duang, C. Zie, W. Cai, C. He, H. Wu, Y. Cao, Macromolecules 42 (2009) 4410–4415;
(b) B.C. Thompson, B.J. Kim, D.F. Kavulak, K. Sivula, C. Mauldin, J.M.J. Fréchet, Macromolecules 40 (2007) 7425–7428;
(c) A.P. Zoombelt, M.A.M. Leenen, M. Fonrodona, Y. Nicolas, M.M. Wienk, R.A.J. Janssen, Polymer 50 (2009) 4564–4570;
(d) C. Piliego, T.W. Holcombe, J.D. Douglas, C.H. Woo, P.M. Beaujuge, J.M.J. Fréchet, J. Am. Chem. Soc. 132 (2010) 7595–7597;
(e) Y. Liang, D. Feng, S.T. Tsai, G. Li, C. Ray, L. Yu, J. Am. Chem. Soc. 131 (2009) 7792–7799;
(f) J.M. Szarko, J. Guo, Y. Liang, B. Lee, B.S. Rolczynski, J. Strzalka, T. Xu, S. Loser, T.J. Marks, L. Yu, L.X. Chen, Adv. Mater. 22 (2010) 5468–5472;
(g) L. Yang, H. Zhou, W. You, J. Phys. Chem. C 114 (2010) 16793–16800.
[7] L. Biniek, S. Fall, C.L. Chochos, D.V. Anokhin, D.A. Ivanov, N. Leclerc, P. Lévêque, T. Heiser, Macromolecules 43 (2010) 9779–9786.
[8] L. Biniek, C.L. Chochos, G. Hadziioannou, N. Leclerc, P. Lévêque, T. Heiser, Macromol. Rapid Commun. 31 (2010) 651–656.
[9] Available from: <http://www.wavefun.com>.
[10] P.N. Murgatroyd, J. Phys. D: Appl. Phys. 3 (1970) 151–156.
[11] H. Zhou, L. Yang, S. Xiao, S. Liu, W. You, Macromolecules 43 (2010) 811–820.
[12] P.M. Beaujuge, S. Ellinger, J.R. Reynolds, Nat. Mater. 7 (2008) 795–799.